Published in final edited form as:
J Thorac Cardiovasc Surg. 2014 March ; 147(3): 1056–1064. doi:10.1016/j.jtcvs.2013.04.028.

Mechanism of Aortic Medial Matrix Remodeling is Distinct in Bicuspid Aortic Valve Patients

Julie A. Phillippi, PhD[a,b,c,d,e], **Benjamin R. Green, MS**[a], **Michael A. Eskay**[a], **Mary P. Kotlarczyk, PhD**[a], **Michael R. Hill, PhD**[f], **Anne M. Robertson, PhD**[g], **Simon C. Watkins, PhD**[h], **David A. Vorp, PhD**[a,b,d,e], and **Thomas G. Gleason, MD**[a,b,c,d,e]

[a]Department of Cardiothoracic Surgery, University of Pittsburgh, Pittsburgh, PA

[b]Department of Bioengineering, University of Pittsburgh, Pittsburgh, PA

[c]Center for Thoracic Aortic Disease, University of Pittsburgh, Pittsburgh, PA

[d]McGowan Institute for Regenerative Medicine, University of Pittsburgh, Pittsburgh, PA

[e]Center for Vascular Remodeling and Regeneration, University of Pittsburgh, Pittsburgh, PA

[f]Institute for Computational Engineering and Sciences, University of Texas, Austin, TX

[g]Department of Mechanical Engineering and Materials Science, University of Pittsburgh, Pittsburgh, PA

[h]Department of Cell Biology and Physiology, University of Pittsburgh, Pittsburgh, PA

Abstract

OBJECTIVES—Patients with bicuspid aortic valve (BAV) are predisposed to developing ascending thoracic aortic aneurysms (TAA) at an earlier age than patients who develop degenerative TAAs and have a tricuspid aortic valve (TAV). The hypothesis tested is that BAV-associated aortopathy is mediated by a mechanism of matrix remodeling that is distinct from that seen in TAAs of TAV patients.

METHODS—Aortic specimens were collected during ascending aortic replacement, aortic valve replacement and heart transplants from non-aneurysmal (NA) donors and recipients. Matrix architecture of the aortic media was assessed qualitatively using multi-photon microscopy followed by quantification of collagen and elastin fiber orientation. α-elastin was determined and matrix maturity was assessed by quantifying immature and mature collagen and lysyl oxidase (Lox) expression and activity in aortic specimens. Matrix metalloproteinase (MMP)-2/9 activity was quantified in aortic smooth muscle cells.

RESULTS—Elastin and collagen fibers were more highly aligned in BAV-NA and BAV-TAA patients relative to TAV-TAA patients while TAV-TAA was more disorganized than TAV-NA. α-elastin content was unchanged. Immature collagen was reduced in BAV-NA and BAV-TAA when compared with TAV-NA and TAV-TAA. Mature collagen was elevated in TAV-TAA relative to

Corresponding author: Thomas G. Gleason, MD, C-700 Presbyterian University Hospital, 200 Lothrop St, Pittsburgh, PA 15213, 412-802-8529, gleasontg@upmc.edu.

There are no conflicts of interest to disclose.

TAV-NA and BAV-TAA. There was a trend toward elevated Lox gene expression and activity and MMP-2/9 activity for TAV-TAA, BAV-NA and BAV-TAA specimens.

CONCLUSIONS—The highly aligned matrix architecture in BAV patients indicates that wall remodeling is distinct from TAV-TAA. Altered matrix architecture and reduced collagen maturity suggests that the effector molecules mediating remodeling of TAA are different in BAV and TAV patients.

Introduction

Congenital bicuspid aortic valve (BAV) is associated with an aortopathy manifesting as ascending thoracic aortic aneurysm (TAA) and/or aortic dissection. BAV is the most common congenital heart anomaly and affects 1–2% of the population.[1, 2] Data from large surgical centers, including our own report a BAV occurrence rate of ~40% for patients undergoing aortic replacement due to TAA. BAV is heritable,[1, 3] but the cause is unknown. The mechanism mediating the aortopathy associated with BAV is also not defined, but the pathology is localized distinctly to the ascending thoracic aorta.

A final common pathway of matrix degeneration is shared between aneurysms of the ascending thoracic and abdominal aorta. Increased expression of the degrading matrix metalloproteinases (MMPs) and reduced expression of their counterparts, the tissue inhibitors of matrix metalloproteinases (TIMPs), results in fragmentation of collagen and elastin fibers. Histopathologic observations of cystic medial degeneration (CMD), smooth muscle cell (SMC) loss, lack of inflammatory cells and proteoglycan accumulation are unique to TAAs and suggest that the inciting mechanism of MMP/TIMP imbalance and matrix degeneration differs for ascending thoracic and abdominal aortic aneurysms.

Patients with BAV are at an increased risk of developing TAA at least 10–15 years earlier than patients with TAV. Although the mechanism of action mediating matrix degeneration in BAV-associated aortopathy is unknown, we postulate that SMCs of the BAV aorta possess an inherent defect that causes a material property change in the vessel wall leading to TAA formation. We previously demonstrated that the oxidative stress response is compromised in SMCs in BAV patients.[4] We recently reported altered biomechanical strength of the vessel wall between BAV and TAV patients. [5] (Pichamuthu *et al*., submitted[6]) These data led us to hypothesize that TAAs arise in BAV and TAV patients by unique mechanisms of matrix remodeling. To test this hypothesis, collagen and elastin matrix architecture and maturity was qualitatively and quantitatively studied in human thoracic aorta from patients with and without aortic aneurysm. We found that BAV and TAV patients exhibit distinctly different aortic matrix architecture suggesting distinct mechanisms of aortic wall remodeling in the two populations.

Methods

Patient selection and specimen acquisition

Ascending thoracic aortic specimens were collected during elective surgery for ascending aortic replacement and/or aortic valve replacement from patients with BAV or tricuspid aortic valve (TAV) with IRB approval and informed patient consent. Specimens were also collected from heart transplant donors and recipients with TAV and absence of aortic disease with approval from the Center for Organ Recovery and Education or IRB approval and informed patient consent, respectively. Patient demographics of sex, age, maximal orthogonal aortic diameter, degree of aortic insufficiency and stenosis and history of hypertension and cigarette smoking were documented (Table 1). TAA patients enrolled in our tissue bank with BAV (median age= 53, n=142) presenting for elective surgery at the University of Pittsburgh Medical Center for ascending aortic replacement do so at least 10

years earlier than patients with TAV (median age=63, n=99). Specimens chosen for each experiment were diameter-matched (median diameters within 2 mm) for TAV-TAA and BAV-TAA patients and ages span the distribution given above. Specimens of both sexes were included in the study.

Upon excision, the specimens were placed in ice-cold saline and transported to the laboratory. A portion of tissue was processed for isolation of primary aortic SMC cultures as previously described.[4, 7].

Multi-photon microscopy of aortic matrix architecture

A 1 cm^2 portion of the specimen was dissected, noting proximal/distal orientation. The adventitia was left intact to avoid potential deformation in the native matrix architecture. The specimen was kept in PBS on ice and imaged immediately (within 2 hr of harvest) using multi-photon microscopy (MPM) or fixed in 2% paraformaldehyde for 1 hr, followed by storage in PBS at 4°C until MPM was performed. Specimens were imaged using an Olympus FV1000 MPE (Tokyo, Japan) equipped with a Spectra-Physics DeepSee Mai Tai Ti-Sapphire laser (Newport, Mountain View, CA) using an excitation wavelength of 830 nm and 1.12 NA 25X MPE water immersion objective. Epi-detectors were utilized to collect the second harmonic generation at 400±50 nm for collagen fibers and autofluorescence of elastin at 525±25 nm. Images were captured using a dwell time of 4 μs/pixel and a Kalman filter of 2. Images of the media were captured as 2 μm slices starting just beyond the intimal surface sequentially moving towards the adventitia. An attempt to capture images spanning the full thickness of the medial layer was made with each specimen; however, the number of images collected varied with each sample due to thickness and geometry of the specimen and ranged from 14–108 μm.

Determination of collagen and elastin fiber alignment

Following MPM analysis, projected image stacks were assembled for each channel (collagen and elastin separately) using ImageJ (National Institutes of Health). To quantify collagen and elastin fiber orientation on superimposed 2D image stacks, the gradient of image intensity at each pixel taken above a threshold, was determined for an edge detection algorithm using a custom MATLAB program previously described. [8] Briefly, these values were entered into an accumulator bin defined over a subregion and for each angle the summed gradient-weighted contribution of each pixel was calculated. Histograms of dominant orientation, defined as the angle associated with the maximum accumulator bin value were plotted, and orientation indices (OI) were determined based on variance of fiber angle ($\Delta\theta$) of 50% of the total number of fibers as one-half the area under the curve of fiber angle distribution histogram (Figure 2D). For images with a high degree of fiber alignment, it was necessary to rotate the image clockwise 90° to generate half-area calculations from fiber-count angle histograms. The normalized orientation index (NOI) was then calculated from Equation 1 (Eq. 1) as described previously[9] where OI=$\Delta\theta$.

$$\mathrm{NOI}=90-\mathrm{OI}/90\times 100\,\mathrm{so\,that\,NOI}\in[0,100] \quad \text{(Eq. 1)}$$

RNA isolation and quantitative real-time PCR

A portion of each specimen was placed in RNA*later* (Life Technologies, Carlsbad, CA) and stored at −20°C until use. Total RNA was isolated using the RNeasy Plus kit (Qiagen, Valencia, CA). Gene expression of *Lysyl oxidase* (*Lox*) was quantified by real-time PCR as previously described[7] using the One-Step Taqman® PCR kit and custom-designed Taqman® gene expression assay for human *Lox* (Assay ID# Hs00184700_m1) (Life Technologies).

Histology

Specimens (~0.5 × 1cm^2) were fixed in 10% buffered formalin and paraffin embedded. Four micron sections were stained using Masson's Trichrome and Verheoff's van Giemsa (Research Histology Services, University of Pittsburgh Thomas E. Starzl Transplantation Institute) to ascertain collagen and elastin composition respectively. Slides were stained using picrosirius red stain kit (Polysciences Inc., Warrington, PA) according to the manufacturer's instructions to assess collagen fiber thickness. Slides were visualized using a Nikon TE-2000-E inverted microscope under polarized light and captured using a Nikon DS-Fi1 5MP color camera and NIS Elements Software 3.2 (Nikon Corporation, Melville, NY). Mean area fractions of red/orange and green fibers were quantified.

Determination of soluble and insoluble collagen

Snap-frozen aortic specimens were pulverized under liquid nitrogen and weighed. Pepsin-soluble collagen was extracted using 5mg/mL pepsin in 0.5M glacial acetic acid (20 μL/g tissue) overnight at 4°C. Samples were centrifuged at 2,100 × *g* for 6 min at RT. Undenatured soluble "immature" collagen was detected from the supernatant fraction using the Sircol™ assay according to the manufacturer's instructions and a standard curve of Type I collagen (Accurate Chemical and Scientific Corporation, Westbury, NY) and normalized to tissue mass.

Insoluble collagen content was estimated from the pellet fraction following pepsin digestion using a colorimetric hydroxyproline (HYP) assay.[10] Pelleted samples with a minimal volume (<10 μL) of pepsin solution were lyophilized, massed and flame-sealed in 10mm Pyrex tubes with 100 μl of 6N HCl containing 0.5% (v/v) phenol. Samples were incubated at 110°C for 24 hr and dried under vacuum. Samples were re-suspended in 1% (v/v) HCl, incubated at 50°C, and an equivalent amount of NaOH. Detection of HYP was achieved by addition of 0.056M Chloramine T for 25 min at RT. Freshly-prepared 1M Ehrlich's reagent was added followed by incubation at 65°C for 20 min. HYP content was estimated from a standard curve of freshly-prepared HYP (Sigma, St. Louis, MO). Absorbance was measured at 550nm in a spectrophotometer (SpectraMax M2, Model# D02667, Molecular Devices, LLC, Sunnyvale, CA) in duplicate wells. HYP values were normalized to the starting mass of the insoluble pellet.

Determination of elastin content

Insoluble α-elastin content was determined from aortic specimens using the Fastin™ Elastin assay (Accurate Chemical and Scientific Corporation) according to the manufacturer's instructions. Tissue samples were pulverized under liquid nitrogen and weighed. Samples were incubated in 750 μL of 0.25M oxalic acid in a 100°C heating block for 1 hr. Samples were brought to RT and centrifuged at 9,300 × *g* for 10 min. The supernatant was digested a second time. Alpha-elastin content was estimated from pooled supernatants using a standard curve of α-elastin and normalized to weight of the tissue.

Determination of Lox and MMP-2/9 activity

For quantification of Lox and MMP 2/9 activity, primary SMCs (passage 4–5) were plated (5,000 cells/cm^2) in SMC growth medium (Cell Applications, San Diego, CA). Media was replenished every other day and conditioned medium was collected after 7 days. Samples were assayed using the Amplite™ Fluorometric Lysyl Oxidase Assay Kit (AAT Bioquest, Sunnyvale, CA) or the Innozyme™ Gelatinase (MMP-2/9) Activity Assay Kit (EMD Millipore, Billerica, MA) according the manufacturers' instructions and reported as fluorescence units normalized to total protein of the conditioned media.

Statistical analyses

Data reported represent mean ± standard error of the mean (SEM) of all experiments performed. A one-way analysis of variance (ANOVA) was performed followed by Fisher's LSD post-hoc test to determine differences among patient groups using SPSS 19.0 software (SYSTAT Software, Inc, Chicago, IL). A Student's T test was used to determine diameter matching for TAV-TAA and BAV-TAA within experiments.

Results

MPM of the ascending thoracic aorta revealed matrix architecture that was unique for BAV and TAV patients (Figure 1, left panel). Collagen and elastin fiber architecture appeared to be organized randomly in TAV-TAA patients versus highly aligned for BAV-NA and BAV-TAA patients when compared with TAV-NA. These observations are reflected in the fiber angle count histograms as relatively sharp peaks (parallel, high alignment) for TAV-NA, BAV-NA and BAV-TAA or shallow peaks (random, low alignment) for TAV-TAA and are displayed in Figure 1 for collagen and elastin fibers (right panel). Quantification of matrix architecture as a measure of NOI (Figure 2A–D) revealed less elastin fiber alignment for TAV-TAA relative to TAV-NA ($p=0.053$) (Figure 2E). A similar trend was observed for collagen ($p=0.115$) (Figure 2F).

The matrix architecture of the BAV aorta was striking. In contrast to TAV-TAA patients, BAV-TAA patients exhibited a highly oriented fiber architecture that was reminiscent of the architecture observed for a normal aorta with respect to distribution of fiber angle alignment (Figure 1). Elastin fiber alignment in BAV-TAA was increased above not only TAV-TAA patients, but also TAV-NA patients ($p<0.001$) (Figure 2E). A similar relationship was determined for the elastin NOI of BAV-NA patients when compared with TAV-NA ($p=0.012$) and TAV-TAA ($p<0.001$). Collagen NOI was increased in BAV-NA ($p=0.009$) and BAV-TAA ($p=0.037$) when compared with TAV-TAA (Figure 2F). Predominant valve pathology (AS or AI) or BAV cusp fusion morphology (Right-Left, Right-Non-coronary or True bicuspid) did not impact collagen or elastin NOIs for BAV-TAA (data not shown). Collagen NOI was reduced with increasing aortic diameter for BAV-TAA patients ($R^2=0.73$) but not for TAV-TAA ($R^2=0.007$). There was no correlation between elastin NOI and aortic diameter for TAV-TAA ($R^2= 0.26$) and BAV-TAA patients ($R^2=0.002$). Our findings of distinct patterns of collagen and elastin matrix architecture in the aortas of BAV and TAV patients led us to question whether differences in matrix protein maturity exist in BAV and TAV aortas.

Histological analyses of aortic specimens confirmed CMD, elastin fragmentation, and collagen disorganization in TAA specimens irrespective of aortic valve morphology (Figure 3A). Non-uniform collagen distribution, elastin fragmentation and CMD were observed for TAV-TAA, BAV-NA and BAV-TAA.

There was no difference in α-elastin content among the patient groups ($p>0.2$) (Figure 3B). To assess collagen maturity, soluble collagen "newly synthesized, immature" and insoluble "cross-linked, mature" collagen was quantified. Immature collagen was reduced in BAV-NA and BAV-TAA specimens when compared with TAV-NA and TAV-TAA (Figure 3C) ($p<0.02$) and unchanged between TAV-NA and TAV-TAA ($p=0.826$). There was an elevated amount of mature collagen in TAV-TAA relative to TAV-NA and BAV-TAA ($p<0.03$) (Figure 3D). Mature collagen appeared to be increased in BAV-NA relative to normal ($p=0.105$). Qualitative (Figure 4A) and quantitative (Figure 4B) image analysis of picrosirius red stained sections for each color representing thick (red) and thin (green) fibers suggested there was an increased amount of thicker diameter collagen for TAV-TAA when

compared to TAV-NA and BAV-TAA similar to that of insoluble, mature collagen (Figure 3D).

To estimate cross-linking capability, *Lox* gene expression was quantified and revealed a trend of elevated mRNA in TAV-TAA, BAV-NA and BAV-TAA patients (p=0.079) (Figure 5A), but there was an equivalent level of LOX enzyme activity among all groups (p=0.999) (Figure 5B). MMP-2/9 activity appeared to be elevated in TAV-TAA, BAV-NA and BAV-TAA SMCs when compared to TAV-NA (p=0.189) (Figure 5C). Gelatin zymography for active MMP-2 yielded similar pattenr (data not shown).

Discussion

The hallmarks of TAAs in BAV and TAV patients are CMD, elastin fragmentation and smooth muscle cell loss. However, TAAs of BAV and TAV patients are histologically indistinguishable from one another and exhibit patient-to-patient variability in matrix organization. Consequently, characterization of valve-specific pathology is difficult. There are disparate reports in the literature on collagen content in various aortopathies. Some reported increased collagen content in thoracic aortic dissections [11, 12] and AAA[13, 14] while others reported no change in collagen for Marfan-related TAA and AAA[15] or BAV-associated TAA.[16] Spatially-dependent reductions in collagen have been described for patients with BAV-TAA.[17] We previously observed elevated *Type I* collagen mRNA levels in BAV-TAA versus normal patients,[7] and found total collagen content to be unchanged in BAV-TAA when compared to TAV-TAA (Pichamuthu, *et al.*, submitted[6]). We demonstrate here similar elastin content among all patient groups. Hence, there may be a consensus that differences in BAV vs. TAV-associated TAA cannot be reconciled by biochemical changes in the amount of collagen and elastin.

To identify differences in aortic matrix micro-architecture between BAV and TAV patients, we focused our efforts on a qualitative and quantitative interrogation of collagen and elastin architecture. Other reports have examined aortic matrix architecture in human and animal models using electron microscopy,[18, 19] a time consuming and destructive process with opportunities for introduction of artifact and screening error. MPM has the capability of visualizing collagen and elastin distinctly in freshly-isolated native tissue with minimal, nondestructive processing. We employed MPM to interrogate aortic matrix architecture in human aortic specimens from non-aneurysmal and aneurysmal BAV and TAV patients. The differences in collagen and elastin fiber architecture were striking. TAV-TAA patients demonstrated a random, multi-directional organization of collagen and elastin. In contrast, we discovered that BAV patients displayed a highly aligned uni-directional and parallel fiber architecture. Our findings are consistent with others who proposed that defects in collagen microarchitecture underlie the pathology of thoracic aortic aneurysms related to Marfan syndrome.[15] Interestingly, the aorta of AAA and Marfan patients was also reported to be stiffer than normal[20, 21] presumably due to a greater proportion of aligned collagen fibrils.[15]

The notion of a “microstructural malfunction” rather than a collagen deficit mediating aneurysm formation has been proposed for Marfan-related TAA.[15] The stark differences in collagen and elastin fiber architecture in BAV vs. TAV patients indicate that BAV aortopathy involves a remodeling process distinct from that which occurs in aneurysms of TAV patients. Given that BAV-NA patients also exhibited the same highly aligned fiber orientation as BAV-TAA patients, suggests remodeling to be an early event, even before aortic dilatation. These BAV-NA patients have clinical aortic valve disease and various degrees of aortic stenosis and/or insufficiency (Table 1). Matrix remodeling in BAV patients to a more highly aligned fiber architecture appears to be an inherent, early response perhaps

as an adaptation to the molecular pathology and/or turbulent systolic flow jets through the BAV. [22] The highly-oriented collagen fibers may account for our observed differences in vessel strength between TAV-TAA and BAV-TAA[5](Pichamuthu *et al*., submitted[6]) as aligned collagen fibers tend to be stiffer than randomly oriented fibers,[23, 24] and BAV patients exhibit increased stiffness of the ascending aorta irrespective of dilatation.[25, 26] Realignment of collagen fibers has been shown to be driven by cell orientation[27] supporting our seminal hypothesis that remodeling during TAA in the BAV patient is cell-mediated.[4] Furthermore, the recognition of highly aligned elastin fibers is consistent with the known reduced elasticity of BAV-aorta.[26] The logarithm for determination of collagen and elastin fiber orientation was previously applied to studies of stress-mediated collagen fiber recruitment in rabbit carotid arteries.[8] Our results follow a similar premise in that collagen fiber alignment in BAV patients may constitute a remodeling mechanism in response to circumferential load-bearing that contributes to stress-mediated mechanical stiffening of the vessel.[28] Collagen fibers were less aligned with increasing aortic diameter for BAV-TAA but not TAV-TAA, suggesting a secondary remodeling mechanism in BAV patients during progressive dilatation that could potentially be due to local variations in wall stress[29] and warrants further study. BAV patients may have an inability to continually compensate for ongoing degeneration with increasing pressure on the vessel with dilatation. The uniquely remodeled architecture and altered biomechanical responses in BAV and TAV patients[5] (Pichamuthu, *et al.*, submitted[6]) suggest that different effectors lead to microstructural defects that govern the remodeling process.

Our finding of reduced immature collagen in BAV patients relative to TAV patients and irrespective of aortic diameter supports altered collagen remodeling mechanisms at play in the BAV-associated aortopathy. Less immature collagen is consistent with the established pattern of increased MMP activity in BAV-associated TAAs[16, 30, 31] confirmed here in SMCs from TAV-TAA, BAV-NA and BAV-TAA patients, since immature, non-cross-linked collagen is more susceptible to proteolysis. An alternative explanation is that reduced immature collagen in BAV patients could be the result of decreased post-transcriptional modifications and/or increased pre-pro-collagen protein turnover since we previously observed elevated Type I collagen mRNA expression in BAV-TAA patients.[7] Mature collagen was increased in TAV-TAA patients when compared with TAV-NA and BAV-TAA patients, suggesting a collagen remodeling response in TAV-TAA patients that is lacking in BAV patients. Normal levels of immature collagen in TAV-TAA despite elevated MMP activity also points to an altered collagen remodeling response in BAV vs. TAV patients. Assessment of collagen fiber diameter via picrosirius red staining concurred with our biochemical analysis of insoluble collagen but did not indicate collagen fiber diameter to be a prominent microstructural alteration for BAV patients.

These differences in collagen maturity and architecture appear to be independent from cross-linking as *Lox* gene expression seemed to be elevated similarly in pathologic specimens. The elevated *Lox* mRNA pattern was congruent to that of Type I collagen, further suggesting that the transcriptional machinery responsible for collagen and Lox expression is over-stimulated by the same unknown mechanism. Our results complement others who found that Lox and Type I collagen were elevated in patients with Marfan syndrome[15] and postulated the involvement of TGF-β in this connective tissue disorder. [32] TGF-β1 is known to regulate *Collagen* and *Lox* expression and govern post-transcriptional and post-translational processing of LOX. [33] However, the role of TGF-β in BAV aortopathy needs to be further investigated.

These data collectively lead us to propose that the BAV aorta remodels by a unique mechanism distinct from that giving rise to TAA in TAV patients. These alterations in matrix architecture in BAV aorta are evident prior to dilatation and well before the typically

recommended point of surgical intervention which is when the aortic diameter reaches a maximal orthogonal measurement between 50–55 mm. It is reasonable to surmise that with an increased understanding of the role matrix fiber alignment and architecture plays in the biomechanical stability of the vessel wall, improved risk assessments for development of TAA and life-threatening dissections can be attained. Further study on the direct impact of the distinct pattern of matrix remodeling in BAV patients described here on the underlying known differences in biomechanical strength, the putative cell-mediated mechanisms governing the remodeling process and consideration of the effects of disrupted hemodynamics specific to the pattern of BAV cusp fusion will help glean new insight towards identifying the relative risk for aortic catastrophe in BAV patients. Interrogation of fetal and pediatric specimens could offer insight on the timing of matrix remodeling and whether the process is adaptive or the distinct differences in architecture are congenital. Ongoing efforts in our laboratory are targeted on characterization of the effector molecules governing the matrix remodeling process in BAV-associated aortopathy.

Study Limitations

Due to the relatively small portion of tissue that is able to be excised from non-aneurysmal patients with BAV during elective aortic valve replacement, the number of assays that can be performed per patient were limited and this resulted in lower sample sizes for this cohort. The TAV-NA group had appreciably less instances of AI and no instances of AS due to the majority of this patient cohort being comprised of normal “healthy” organ donors, making inferences on the impact of aortic valve pathology on study outcomes difficult.

Acknowledgments

Funding source: The National Heart, Lung and Blood Institute of the National Institutes of Health, award # HL109132 to Dr. Thomas Gleason and the University of Pittsburgh Medical Center.

Research reported in this publication was supported by the National Heart, Lung and Blood Institute of the National Institutes of Health under Award Number RO1HL109132 (TG). The authors gratefully acknowledge Erica Butler, Kristin Valchar and Julie Schreiber for assistance with IRB protocols and informed patient consent, Deborah Cleary and Dr. John Hempel for assistance with the hydroxyproline assay, Jalice Shedrick for assistance with picrosirius red staining, Dr. Antonio D’Amore for helpful discussions on calculating fiber orientation, and Gregory Gibson for assistance with multi-photon microscopy. We thank Drs. Christian Bermudez, Jay Bhama, Forozan Navid, and Lawrence Wei of the Department of Cardiothoracic Surgery, University of Pittsburgh Medical Center for aortic specimen acquisition. We also gratefully acknowledge the assistance of Dr. Phil Campbell for helpful discussions on data analysis and review of statistical analyses.

References

1. Gleason TG. Heritable disorders predisposing to aortic dissection. Semin Thorac Cardiovasc Surg. 2005; 17:274–81. [PubMed: 16253833]
2. Ward C. Clinical significance of the bicuspid aortic valve. Heart. 2000; 83:81–5. [PubMed: 10618341]
3. Cripe L, Andelfinger G, Martin LJ, Shooner K, Benson DW. Bicuspid aortic valve is heritable. Journal of the American College of Cardiology. 2004; 44:138–43. [PubMed: 15234422]
4. Phillippi JA, Klyachko EA, Kenny JPt, Eskay MA, Gorman RC, Gleason TG. Basal and oxidative stress-induced expression of metallothionein is decreased in ascending aortic aneurysms of bicuspid aortic valve patients. Circulation. 2009; 119:2498–506. [PubMed: 19398671]
5. Pasta S, Phillippi JA, Gleason TG, Vorp DA. Effect of aneurysm on the mechanical dissection properties of the human ascending thoracic aorta. J Thorac Cardiovasc Surg. 2011
6. Pichamuthu, J.; Phillippi, JA.; Cleary, DA.; Chew, DW.; Hempel, J.; Vorp, DA.; Gleason, TG. Differential Tensile Strength Profiles and Collagen Constructs in Ascending Aortic Aneurysms by Aortic Valve Phenotype. (submitted)

7. Phillippi JA, Eskay MA, Kubala AA, Pitt BR, Gleason TG. Altered oxidative stress responses and increased type I collagen expression in bicuspid aortic valve patients. Ann Thorac Surg. 2010; 90:1893–8. [PubMed: 21095332]
8. Hill MR, Duan X, Gibson GA, Watkins S, Robertson AM. A theoretical and non-destructive experimental approach for direct inclusion of measured collagen orientation and recruitment into mechanical models of the artery wall. Journal of biomechanics. 2012; 45:762–71. [PubMed: 22305290]
9. D'Amore A, Stella JA, Wagner WR, Sacks MS. Characterization of the complete fiber network topology of planar fibrous tissues and scaffolds. Biomaterials. 2010; 31:5345–54. [PubMed: 20398930]
10. Stegemann H, Stalder K. Determination of hydroxyproline. Clin Chim Acta. 1967; 18:267–73. [PubMed: 4864804]
11. de Figueiredo Borges L, Jaldin RG, Dias RR, Stolf NA, Michel JB, Gutierrez PS. Collagen is reduced and disrupted in human aneurysms and dissections of ascending aorta. Hum Pathol. 2008; 39:437–43. [PubMed: 18261628]
12. Wang X, LeMaire SA, Chen L, Shen YH, Gan Y, Bartsch H, Carter SA, Utama B, Ou H, Coselli JS, Wang XL. Increased collagen deposition and elevated expression of connective tissue growth factor in human thoracic aortic dissection. Circulation. 2006; 114:I200–5. [PubMed: 16820572]
13. Menashi S, Campa JS, Greenhalgh RM, Powell JT. Collagen in abdominal aortic aneurysm: typing, content, and degradation. J Vasc Surg. 1987; 6:578–82. [PubMed: 2826827]
14. Rizzo RJ, McCarthy WJ, Dixit SN, Lilly MP, Shively VP, Flinn WR, Yao JS. Collagen types and matrix protein content in human abdominal aortic aneurysms. J Vasc Surg. 1989; 10:365–73. [PubMed: 2795760]
15. Lindeman JH, Ashcroft BA, Beenakker JW, van Es M, Koekkoek NB, Prins FA, Tielemans JF, Abdul-Hussien H, Bank RA, Oosterkamp TH. Distinct defects in collagen microarchitecture underlie vessel-wall failure in advanced abdominal aneurysms and aneurysms in Marfan syndrome. Proc Natl Acad Sci U S A. 2010; 107:862–5. [PubMed: 20080766]
16. Fedak PW, de Sa MP, Verma S, Nili N, Kazemian P, Butany J, Strauss BH, Weisel RD, David TE. Vascular matrix remodeling in patients with bicuspid aortic valve malformations: implications for aortic dilatation. J Thorac Cardiovasc Surg. 2003; 126:797–806. [PubMed: 14502156]
17. Della Corte A, Quarto C, Bancone C, Castaldo C, Di Meglio F, Nurzynska D, De Santo LS, De Feo M, Scardone M, Montagnani S, Cotrufo M. Spatiotemporal patterns of smooth muscle cell changes in ascending aortic dilatation with bicuspid and tricuspid aortic valve stenosis: focus on cell-matrix signaling. J Thorac Cardiovasc Surg. 2008; 135:8–18. 18, e1–2. [PubMed: 18179910]
18. Raspanti M, Protasoni M, Manelli A, Guizzardi S, Mantovani V, Sala A. The extracellular matrix of the human aortic wall: ultrastructural observations by FEG-SEM and by tapping-mode AFM. Micron. 2006; 37:81–6. [PubMed: 16081297]
19. Ushiki T. Collagen fibers, reticular fibers and elastic fibers. A comprehensive understanding from a morphological viewpoint. Archives of histology and cytology. 2002; 65:109–26. [PubMed: 12164335]
20. He CM, Roach MR. The composition and mechanical properties of abdominal aortic aneurysms. J Vasc Surg. 1994; 20:6–13. [PubMed: 8028090]
21. Sonesson B, Hansen F, Lanne T. Abnormal mechanical properties of the aorta in Marfan's syndrome. European journal of vascular surgery. 1994; 8:595–601. [PubMed: 7813727]
22. Hope MD, Hope TA, Meadows AK, Ordovas KG, Urbania TH, Alley MT, Higgins CB. Bicuspid aortic valve: four-dimensional MR evaluation of ascending aortic systolic flow patterns. Radiology. 2010; 255:53–61. [PubMed: 20308444]
23. Brown RA, Prajapati R, McGrouther DA, Yannas IV, Eastwood M. Tensional homeostasis in dermal fibroblasts: mechanical responses to mechanical loading in three-dimensional substrates. J Cell Physiol. 1998; 175:323–32. [PubMed: 9572477]
24. Lo CM, Wang HB, Dembo M, Wang YL. Cell movement is guided by the rigidity of the substrate. Biophys J. 2000; 79:144–52. [PubMed: 10866943]

25. Bilen E, Akcay M, Bayram NA, Kocak U, Kurt M, Tanboga IH, Bozkurt E. Aortic elastic properties and left ventricular diastolic function in patients with isolated bicuspid aortic valve. The Journal of heart valve disease. 2012; 21:189–94. [PubMed: 22645854]
26. Nistri S, Grande-Allen J, Noale M, Basso C, Siviero P, Maggi S, Crepaldi G, Thiene G. Aortic elasticity and size in bicuspid aortic valve syndrome. European heart journal. 2008; 29:472–9. [PubMed: 18096569]
27. Wang JH, Jia F, Gilbert TW, Woo SL. Cell orientation determines the alignment of cell-produced collagenous matrix. Journal of biomechanics. 2003; 36:97–102. [PubMed: 12485643]
28. Okamoto RJ, Xu H, Kouchoukos NT, Moon MR, Sundt TM 3rd. The influence of mechanical properties on wall stress and distensibility of the dilated ascending aorta. J Thorac Cardiovasc Surg. 2003; 126:842–50. [PubMed: 14502164]
29. Nathan DP, Xu C, Plappert T, Desjardins B, Gorman JH 3rd, Bavaria JE, Gorman RC, Chandran KB, Jackson BM. Increased ascending aortic wall stress in patients with bicuspid aortic valves. Ann Thorac Surg. 2011; 92:1384–9. [PubMed: 21867987]
30. Ikonomidis JS, Jones JA, Barbour JR, Stroud RE, Clark LL, Kaplan BS, Zeeshan A, Bavaria JE, Gorman JH 3rd, Spinale FG, Gorman RC. Expression of matrix metalloproteinases and endogenous inhibitors within ascending aortic aneurysms of patients with bicuspid or tricuspid aortic valves. J Thorac Cardiovasc Surg. 2007; 133:1028–36. [PubMed: 17382648]
31. Boyum J, Fellinger EK, Schmoker JD, Trombley L, McPartland K, Ittleman FP, Howard AB. Matrix metalloproteinase activity in thoracic aortic aneurysms associated with bicuspid and tricuspid aortic valves. J Thorac Cardiovasc Surg. 2004; 127:686–91. [PubMed: 15001896]
32. Dietz HC, Cutting GR, Pyeritz RE, Maslen CL, Sakai LY, Corson GM, Puffenberger EG, Hamosh A, Nanthakumar EJ, Curristin SM, et al. Marfan syndrome caused by a recurrent de novo missense mutation in the fibrillin gene. Nature. 1991; 352:337–9. [PubMed: 1852208]
33. Feres-Filho EJ, Choi YJ, Han X, Takala TE, Trackman PC. Pre- and post-translational regulation of lysyl oxidase by transforming growth factor-beta 1 in osteoblastic MC3T3-E1 cells. J Biol Chem. 1995; 270:30797–803. [PubMed: 8530522]

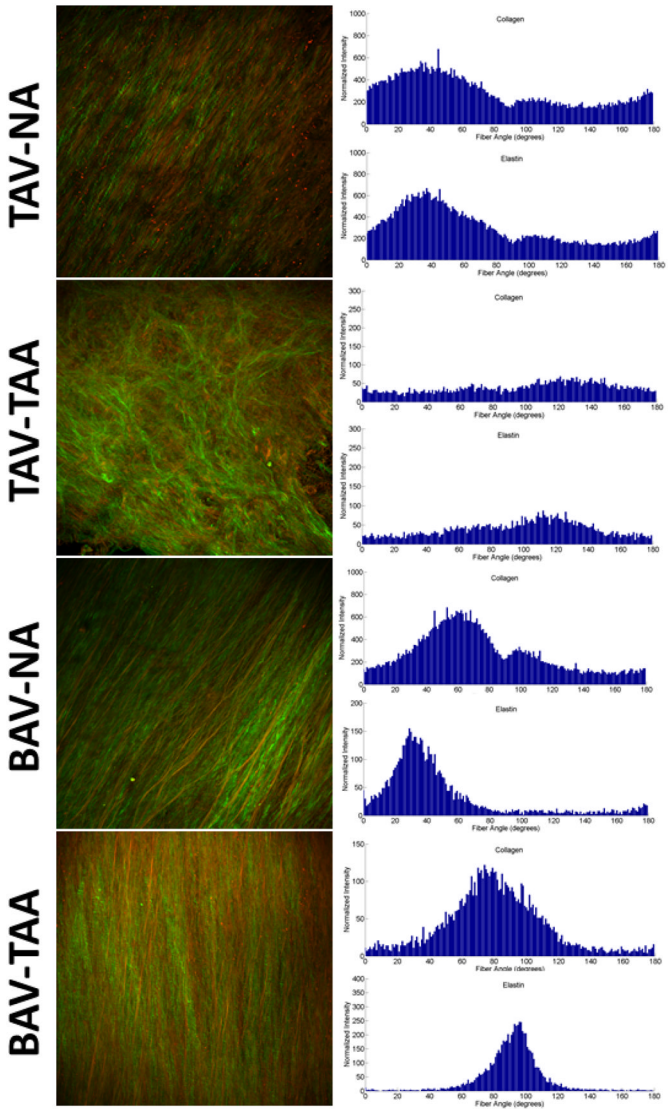

Figure 1.

Matrix architecture of human ascending thoracic aorta. Representative images of collagen (green) and elastin (red) fiber orientation acquired using multi-photon microscopy (left panel). Magnification is 25X. Histograms of collagen and elastin fiber angle counts (right panels).

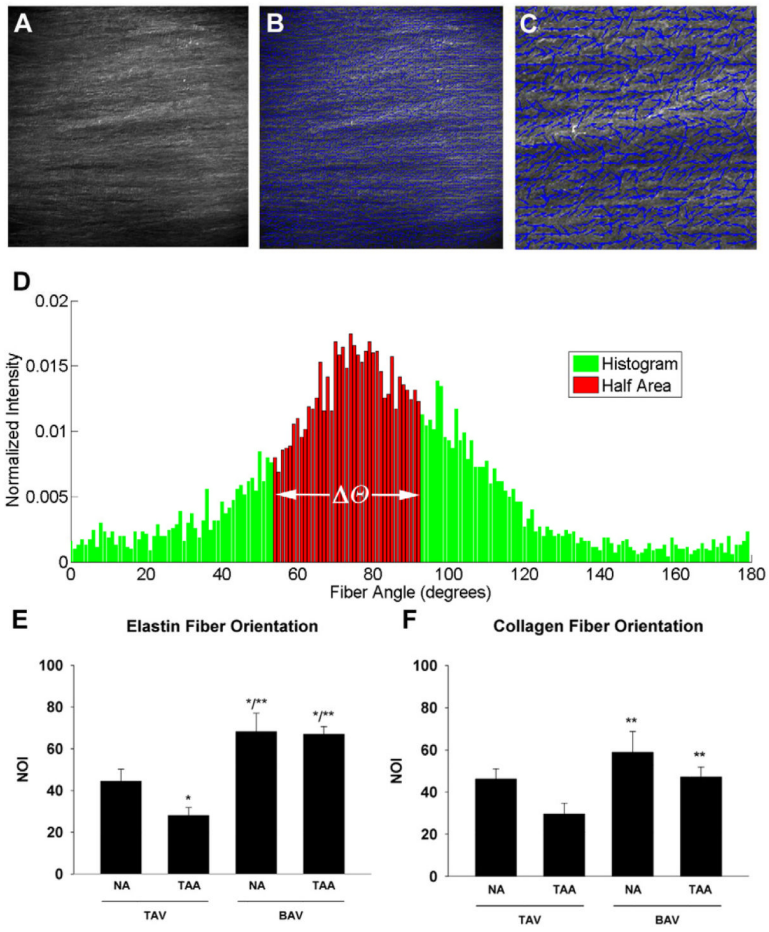

Figure 2.

Determination of matrix fiber orientation. A) Representative monochromatic image of collagen fiber matrix of a BAV-TAA patient using multi-photon microscopy. Magnification is 25X. B) Vector map (blue arrows) of fiber alignment for image in (A). C) Increased magnification of box indicated in (B) to illustrate fiber alignment vectors. D) Representative histogram of collagen fiber angle counts for BAV-TAA generated from multi-photon image in (A) to calculate the orientation index (Δθ). E–F) Normalized orientation indices (NOIs) for elastin and collagen respectively. Bars represent mean ± SEM, n=5 (TAV-NA), 8,9 (TAV-TAA), 6 (BAV-NA) and 10 (BAV-TAA) *Significant from TAV-NA, ** Significant from TAV-TAA, $p<0.05$.

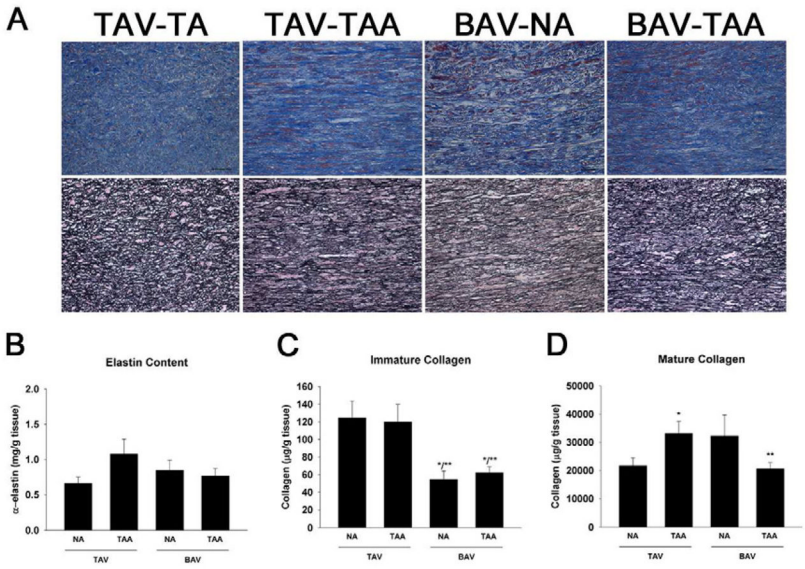

Figure 3.

Assessment of matrix composition and maturity. A) Verhoeff's van Giemsa (top panel) and Masson's trichrome (bottom panel) for representative ascending thoracic aortic specimens. Images were oriented such that the adventitial side is located at the top and intimal side on the bottom. Images were captured at 20X magnification. Scale bar= 50 μm. B) Elastin content, n=10 (TAV-NA), 9 (TAV-TAA), 5 (BAV-NA) and 11 (BAV-TAA). C) Immature collagen n=8 (TAV-NA), 9 (TAV-TAA), 4 (BAV-NA) and 9 (BAV-TAA) and D) Mature collagen n=8 (TAV-NA), 7 (TAV-TAA), 3 (BAV-NA) and 8 (BAV-TAA) and bars represent mean ± SEM. *Significant from TAV-NA, **Significant from TAV-TAA, $p<0.05$.

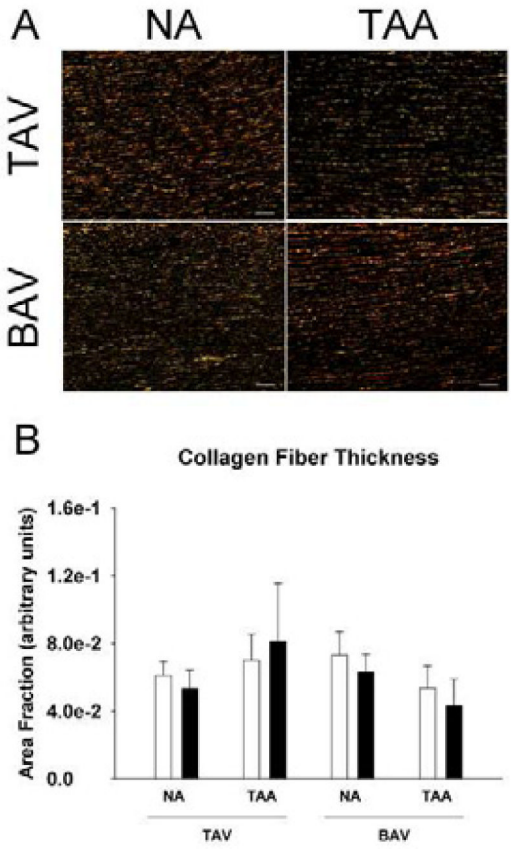

Figure 4.

Picrosirius red staining for collagen fibers in ascending aorta. A) Representative micrographs of aortic specimens imaged using linear polarized light showing thinner (green) and thicker collagen fibers (red). Images were oriented such that the adventitial side is located at the top and intimal side on the bottom. Scale bar=100 μm. B) Quantification of the area fraction of green (open bars) and red (solid bars). Bars represent mean ± SEM, n=3 (TAV-NA), 4 (TAV-TAA) and 5 (BAV-NA, BAV-TAA).

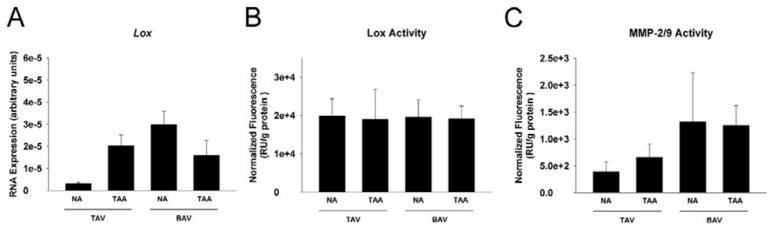

Figure 5.

Lox and MMP analysis. A) *Lox* mRNA expression in aortic tissue specimens n=17 (TAV-NA), 8 (TAV-TAA), 8 (BAV-NA) and 15 (BAV-TAA). B) Lox n=5 (TAV-NA), 4 (TAV-TAA), 3 (BAV-NA) and 15 (BAV-TAA) and C) MMP-2/9 activity n=4 (TAV-NA), 5 (TAV-TAA), 3 (BAV-NA) and 6 (BAV-TAA)

Table 1

All Samples	N (M/F)	Age, yr (Median±S.D.)	Aortic Dia., mm (Median ± S.D.)	HTN% (#/N)	History of Smoking % (#/N)	AI% (#/N)			AS% (#/N)		
						1+	2–3+	4+	Mild	Moderate	Severe
TAV-NA	23 (17/6)	54.0 ±14.9	Normal	39.1% (9/23)	39.1% (9/23)	0% (0/23)	4.5% (1/23)	0% (0/23)	0% (0/23)	0% (0/23)	0% (0/23)
TAV-TAA	26 (22/4)	58.5 ±11.6	52.0 ± 7.1	65.4% (17/26)	23.1% (6/26)	26.9% (7/26)	23.1% (6/26)	15.4% (4/26)	7.7% (2/26)	0% (0/26)	3.8% (1/26)
BAV-NA	15 (11/4)	56.0 ± 14.4	<40	60.0% (9/15)	26.7% (4/15)	13.3% (2/15)	6.7% (1/15)	33.3% (5/15)	0% (0/15)	6.7% (1/15)	53.3% (8/15)
BAV-TAA	39 (35/4)	54.0 ± 9.7	50.0 ± 5.2	41.0% (16/39)	59.0% (23/39)	15.4% (6/39)	23.1% (9/39)	15.4% (6/39)	5.1% (2/39)	10.3% (5/39)	28.2% (11/39)